

## Development of Multiple-Frequency Wireless Coordinative Motor Drives

Chaoqiang Jiang<sup>1, \*</sup>, Kwok Tong Chau<sup>1</sup>, Christopher Ho Tin Lee<sup>2</sup>,  
Wei Han<sup>1</sup>, Wei Liu<sup>1</sup>, and Wong-Hing Lam<sup>1</sup>

**Abstract**—This paper proposes and implements a novel class of inductor-capacitor-capacitor wireless coordinative DC motor drives, which not only performs selective wireless power to motors, but also achieves power equalization to ensure the same operation for isolated robotic arms. The key is to make use of the selective wireless power transfer with several resonant frequencies and then use only one transmitter with the inductor-capacitor-capacitor compensation network to provide multiple-frequency transmission without relying on the switched-capacitor array. In order to provide simultaneous and independent wireless power to different motors and hence achieve the desired coordinative motion, a time-division multiplexing scheme and burst firing control are newly employed. Thus, the wireless power transfer system with multiple receivers can achieve better flexibility and simplicity. Both finite element analysis and experimental results are given to verify the validity of the proposed inductor-capacitor-capacitor wireless coordinative DC motor drive. As a result, the motors can achieve independent motion with 1200 rpm and simultaneous motion with 400 rpm when the torque is 10 Ncm, and the operating frequencies are set at 110 kHz and 130 kHz.

### 1. INTRODUCTION

Since wireless power transfer (WPT) was pioneered by Nikola Tesla, more than one hundred years passed. Until recent decades, the WPT has reattracted substantial attention and becomes one of the most potential technologies [1–3]. Due to the definite advantages of high reliability, high safety, low maintenance, electrical isolation, and better convenience, WPT has been actively developed for various applications [4–6]. So far, the WPT has been successfully commercialized for domestic appliances [7], biomedical devices [8, 9], and electric vehicle (EV) charging [10–12]. Recently, the WPT technique has been extended to emerging applications such as wireless heating [13] and wireless lighting [14]. Especially, the wireless motor shows great potential and commercial value. This is because electric motors are electromechanical energy conversion devices, which account for over 80% electricity consumption [15]. Over the years, their research and development have been focused on improving the efficiency and power density.

However, the portability of electric motors has been a long-term problem because of the need of physical cables or wires. This problem not only limits their flexibility, but also deters their applicability [16, 17]. As the WPT can effectively resolve this problem, it shows great potential for many industrial applications [18–20]. Nevertheless, almost all these applications rely on using WPT to perform battery charging first, and then the charged battery feeds the devices, appliances or vehicles afterwards [21, 22]. By the same token, the wireless motor can readily be derived so that the portability problem of electric motors seems to be solved. However, this is not a real wireless motor, which is

---

*Received 28 December 2018, Accepted 14 February 2019, Scheduled 22 March 2019*

\* Corresponding author: Chaoqiang Jiang (cqjiang@eee.hku.hk).

<sup>1</sup> Department of Electrical and Electronic Engineering, The University of Hong Kong, Pokfulam, Hong Kong, China. <sup>2</sup> School of Electrical & Electronic Engineering, Nanyang Technological University, Singapore.

actually a combination of the wireless battery charging system and the battery-powered motor system. This kind of pseudo-wireless motors suffers from using additional battery, controller and converter, which are bulky, lossy, and costly. Most importantly, it cannot be utilized to work at isolated or inaccessible environment because the battery has a limited cycle life while the controller and converter have a much shorter lifespan than the motor.

In order to address this problem, the wireless reluctance motor and separately excited DC motor drives have been developed to own higher robustness, which do not involve any battery, controller or converter in the motor side [23, 24]. However, these two wireless motor drives introduced two inevitable drawbacks, namely, additional switched capacitor array with high switching voltage and received power differentiation at different operating frequencies. In this paper, the inductor-capacitor-capacitor (LCC) compensation is introduced to solve these two problems and then make this system refrain from using the switched-capacitor array. So far, the LCC compensation network used for multiple-frequency operation is absent in literature.

The purpose of this paper is to propose a novel class of electric motor drives, namely the LCC wireless coordinative DC motor drive. The key is to artfully incorporate selective WPT into the DC motor structure in such a way that each pickup coil is connected to each motor winding via simple rectification, and multiple motor windings can be independently excited and controlled by the same transmitter coil using time-division multiplexing (TDM) and burst firing control (BFC). Furthermore, the LCC compensation is adopted to eliminate the LC tanks and hence achieve received power equalization. Consequently, an array of motors can be wirelessly powered with the same power and independently controlled by the same transmitter, which is highly desirable for some practical applications such as batteryless humanoid robots walking on electrified floors or robotic arms operated in isolated environment.

## 2. SYSTEM CONFIGURATION AND OPERATION

Firstly, the system configuration will be introduced. Two conventional compensation networks, namely the primary series and primary parallel compensations, will be analyzed. Hence, the proposed wireless motor drives with LCC compensation will be presented and analyzed to highlight the advantages of no switched-capacitor array and power equalization for multiple-receiver WPT. Consequently, the system operation principle will be given and realized by using BFC and TDM.

### 2.1. System Configuration

The proposed LCC wireless coordinative motor drive is shown in Figure 1, which includes only one transmitter connected to an LCC compensation network, and two receiver coils that are series compensated by two capacitors with different resonant frequencies. Each receiver feeds a permanent magnet (PM) DC motor via a full wave rectifier consisting of four diodes. According to the magnetic resonant coupling property of WPT, only the receiver that has been tuned at the same operating frequency of the transmitter can pick up the transmitted energy; meanwhile, another receiver which has been tuned to another frequency theoretically cannot pick up any energy.

In Figure 1, it can be found that there is no switched capacitor at the transmitter side to determine the resonant frequency. Thus, the component cost and control complexity are significantly reduced. Furthermore, it should be noted that no battery or power switch is included at the receiver side. Hence, the receiver side does not need any maintenance and can be totally isolated from the transmitter side without any physical contacts.

### 2.2. Conventional Compensation Network Analysis

For the conventional multiple-frequency WPT system as shown in Figure 2, there are two receivers with different resonant frequencies. Generally, the operating frequency of a transmitter should be the same with that of a receiver. Thus, two operating frequencies should be adopted for two receivers with two different resonant frequencies. As a result, a switched capacitor is generally required to achieve multiple-frequency operation.

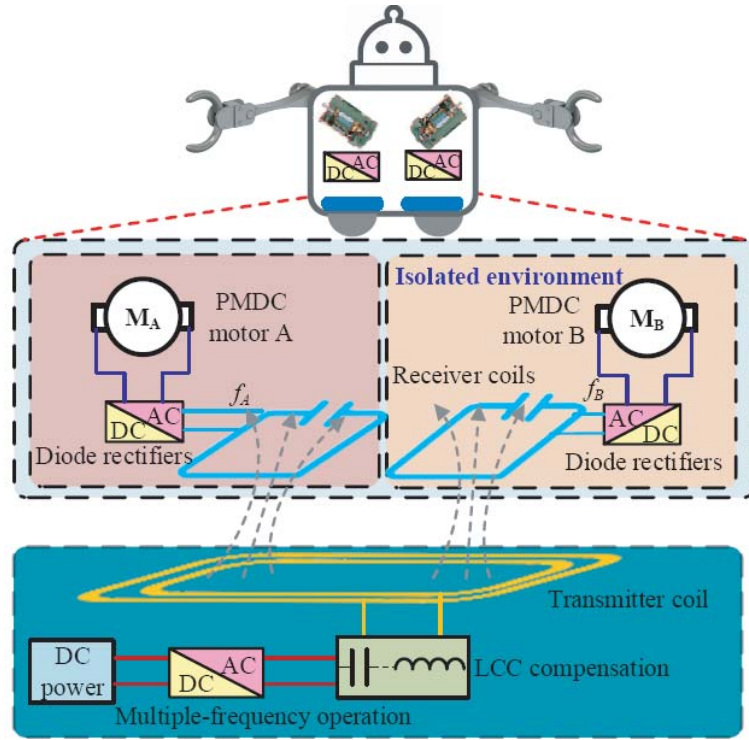


Figure 1. Proposed wireless coordinative DC motor drive.

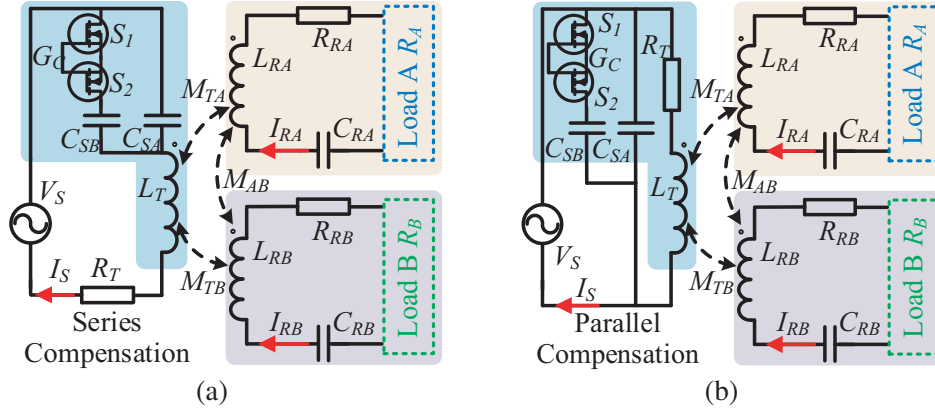


Figure 2. Equivalent circuit of conventional multiple-frequency WPT system. (a) Primary series compensation. (b) Primary parallel compensation.

In a WPT system, both series and parallel compensation networks can be used to reduce the voltage-to-current rating in the coil. Actually, the series compensation is most popularly used at the secondary side. This is because there is no reflected reactance from the secondary side when the operating frequency is set at the resonant frequency of the secondary side [25]. As shown in Figure 2, the primary series and parallel compensation networks are analysed to reveal their shortcomings, where  $V_S$  and  $I_S$  are the AC output voltage and current from a full H-bridge inverter;  $L_T, C_{S_i}$ , and  $R_T$  are the inductance, switched capacitance, and resistance of the transmitter coil ( $i = A, B$ );  $M_{T_i}$  are the mutual inductance between the transmitter and receiver coils, and the mutual inductance  $M_{AB}$  between two receivers is ignored.  $L_{R_i}, C_{R_i}$ , and  $R_{R_i}$  represent the inductance, capacitance, and resistance in the receiver  $i$ . The two reversely connected N-type MOSFETs are used to switch one of the two compensation capacitors, hence achieving two different resonant frequencies.

As shown in Figure 2, there are two receivers with different resonant frequencies  $\omega_A$  and  $\omega_B$ , which can be expressed as

$$\begin{cases} \omega_A = 2\pi f_A = 1/\sqrt{L_{RA}C_{RA}} \\ \omega_B = 2\pi f_B = 1/\sqrt{L_{RB}C_{RB}} \end{cases} \quad (1)$$

Thus, the operating frequencies of the series compensation as shown in Figure 2(a) are

$$\begin{cases} 1/\sqrt{L_T(C_{S1} + C_{S2})} = \omega_A \\ 1/\sqrt{L_T C_{S1}} = \omega_B \end{cases} \quad (2)$$

and the operating frequencies of the parallel compensation as shown in Figure 2(b) are

$$\begin{cases} \frac{1}{C_{S1} + C_{S2}} = \frac{\omega_A^4 M_{TA}^4}{L_T R_A^2} + \omega_A^2 L_T \\ \frac{1}{C_{S1}} = \frac{\omega_B^4 M_{TB}^4}{L_T R_B^2} + \omega_B^2 L_T \end{cases} \quad (3)$$

where the coil resistances are ignored.

Based on the aforementioned equations, the switched capacitances of  $C_{S1}$  and  $C_{S2}$  can be calculated. For a given input current with 110 kHz and 130 kHz, both switching voltage and received current waveforms under two different compensations can be simulated as shown in Figure 3. It can be found that the switching voltages across the switch terminals can reach up to 600 V under the 0.5 A inverter current output, which will bring high voltage stresses to the two switches and thus increase the switching losses. Moreover, the received currents of two receivers are different, namely power disequilibrium will be resulted due to the conventional series and parallel compensations. In order to address the problems of high voltage stress and power disequilibrium, LCC compensation in the primary is desired.

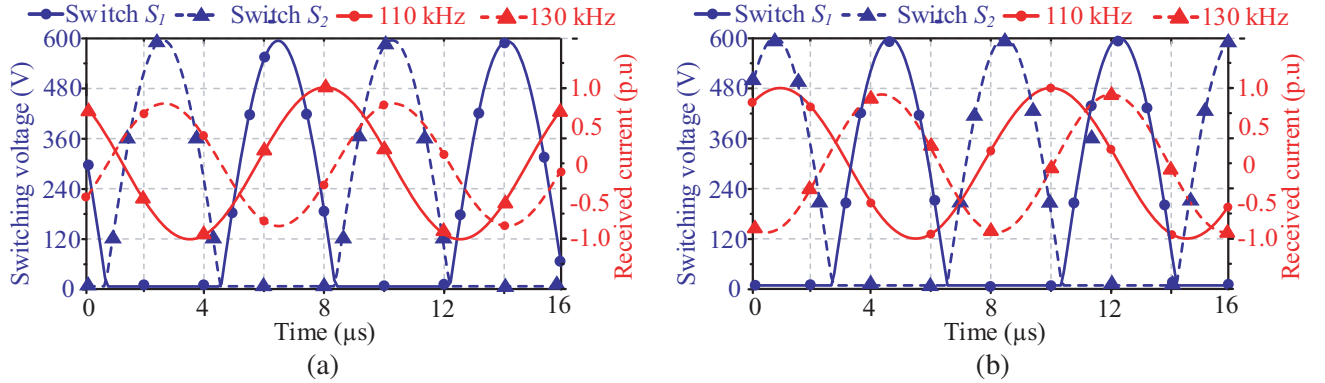


**Figure 3.** Switching voltages and received currents. (a) Primary series compensation. (b) Primary parallel compensation.

### 2.3. LCC Compensation Network Analysis

The equivalent circuit model of the proposed LCC wireless coordinative PMDC motor is shown in Figure 4, where  $L_T$ ,  $C_T$ ,  $R_T$ ,  $I_T$ , and  $I_S$  are the transmitter inductance, transmitter capacitance, transmitter resistance, transmitter coil current, and AC source current, and  $L_{LCC}$  and  $C_{LCC}$  are the inductance and capacitance in the LCC compensation network. The PMDC motor can be equivalently regarded as a resistor  $R_{Mi}$ , a back electromotive force  $E_{mi}$ , and an inductor  $L_{Mi}$  connected in series.  $U_{Ri}$ ,  $U_{Mi}$ ,  $I_{Ri}$ , and  $I_{Mi}$  represent the corresponding voltages and currents before and after the diode rectifier, respectively.

Generally, a PMDC motor can be considered as a variable resistor, which is dependent on the motor speed and load torque. For simplicity, the motor equivalent resistance  $R_{MEq}$  is regarded as a constant

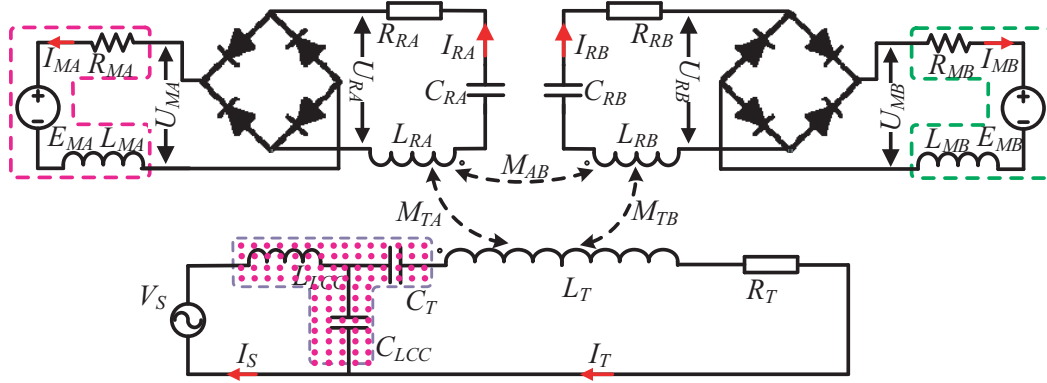


**Figure 4.** Equivalent circuit of proposed LCC wireless coordinative PMDC motor drive.

value due to the constant load torque and speed for fixed robot arm applications. Thus, the equivalent resistance  $R_{DRi}$  before the diode rectifier can be expressed as

$$R_{DRi} = \frac{2\sqrt{2}}{\pi} U_{Mi} / \frac{\pi}{2\sqrt{2}} I_{Mi} = \frac{8}{\pi^2} R_{MEq} \quad (4)$$

Hence, the receivers' impedances  $Z_{RA}$  and  $Z_{RB}$  are given by

$$\begin{cases} Z_{RA} = j\omega L_{RA} + 1/(j\omega C_{RA}) + R_{RA} + R_{DRA} \\ Z_{RB} = j\omega L_{RB} + 1/(j\omega C_{RB}) + R_{RB} + R_{DRB} \end{cases} \quad (5)$$

Referring to the transmitter side, the total reflected impedance  $Z_{Tref}$  from the secondary side can be deduced by dividing the reflected voltage by the primary current so that the  $Z_{Tref}$  from two receivers can be expressed as

$$Z_{Tref} = \frac{-j\omega M_{TA} I_{RA} - j\omega M_{TB} I_{RB}}{I_T} = \frac{\omega^2 M_{TA}^2}{Z_{RA}} + \frac{\omega^2 M_{TB}^2}{Z_{RB}} \quad (6)$$

For each receiver, when the operating frequency is equal to the resonant frequency of receiver  $i$ , the reflected resistance  $\text{Re}(Z_{Trefi})$  and reflected reactance  $\text{Im}(Z_{Trefi})$  can be deduced as

$$\text{Re}Z_{refi} = \frac{\omega_i^4 C_{Ri}^2 M_{Ti}^2 (R_{Ri} + R_{DRi})}{(\omega_i^2 C_{Ri} L_{Ri} - 1)^2 + \omega_i^2 C_{Ri}^2 (R_{Ri} + R_{DRi})^2} = \frac{\omega_i^2 M_{Ti}^2}{R_{Ri} + R_{DRi}} \quad (7)$$

$$\text{Im}Z_{refi} = \frac{-\omega_i^3 C_{Ri} M_{Ti}^2 (\omega_i^2 C_{Ri} L_{Ri} - 1)}{(\omega_i^2 C_{Ri} L_{Ri} - 1)^2 + \omega_i^2 C_{Ri}^2 (R_{Ri} + R_{DRi})^2} = 0 \quad (8)$$

Since the reflected impedance from the untargeted receiver  $i$  is much higher, the total reflected impedance  $Z_{Trefi}$  can be expressed as

$$Z_{Tref} = \frac{\omega_A^2 M_{TA}^2}{R_{RA} + R_{DRA}} \quad \text{or} \quad \frac{\omega_B^2 M_{TB}^2}{R_{RB} + R_{DRB}} \quad (9)$$

Conventionally, LCC compensation network for a single frequency system can provide constant current or voltage operation regardless of the impedance of the load [26]. In this multiple-frequency operation system, constant power should be achieved regardless of the operating frequency variations. The transmitter current  $I_T$  can be calculated by

$$\begin{aligned} I_T &= I_S \frac{(j\omega L_T - j/(\omega C_T) + R_T + Z_{Tref}) \parallel (-j/\omega C_{LCC})}{j\omega L_T - j/(\omega C_T) + R_T + Z_{Tref}} \\ &= V_S \frac{1 - \frac{j\omega L_{LCC}}{Z_S}}{j\omega L_T - j/(\omega C_T) + R_T + Z_{Tref}} \end{aligned} \quad (10)$$

where  $Z_S = j\omega L_{LCC} + \frac{1}{j\omega C_{LCC}} \parallel (j\omega L_T + \frac{1}{j\omega C_T} + R_T + Z_{Tref})$ .

Thus, the received currents of each receiver can be expressed as

$$I_{Ri} = \frac{j\omega_i M_{Ti} I_T}{R_{Ri} + R_{DRi}} \quad (11)$$

And then the power transferred to each motor  $P_i$  can be calculated by

$$P_i = I_{Ri}^2 R_{DRi} \quad (i = A, B) \quad (12)$$

For the proposed LCC wireless coordinative motor system, the receiver A that feeds the PMDC motor A is tuned to the resonant frequency of 110 kHz, whereas the receiver B that feeds the PMDC motor B is tuned to the resonant frequency of 130 kHz. The system parameters are resonant frequencies  $f_j$  of 110 kHz and 130 kHz, transmitter coil resistance  $R_T$  of  $0.8 \Omega$ , receiver coil resistances  $R_{Rj}$  of  $0.4 \Omega$ , mutual inductances  $M_{Tj}$  of  $78 \mu\text{H}$ , transmitter coil inductance  $L_T$  of  $0.79 \text{ mH}$ , receiver coil inductances  $L_{Rj}$  of  $0.50 \text{ mH}$ , LCC inductance  $L_{LCC}$  of  $0.21 \text{ mH}$ , transmitter compensated capacitance  $C_T$  of  $2.7 \text{ nF}$ , and LCC compensated capacitance  $C_{LCC}$  of  $7.3 \text{ nF}$ . When the motor A is targeted, the transmitter should be operated at 110 kHz; when the motor B is targeted, the transmitter should be operated at 130 kHz. Most importantly, the LCC compensated transmitter, without using any switched capacitor array, can provide the same power to different receivers at different resonant frequencies. According to Equations (10)–(12), the received powers of two receivers are plotted in Figures 5(a) and (b) when the motor equivalent resistance is  $25 \Omega$ , namely, the motor is under the torque of  $12 \text{ Ncm}$  and speed of  $1500 \text{ rpm}$ . It can be observed that the power equalization with different operating frequencies can be achieved when the inductance of  $L_{LCC}$  is selected as  $0.21 \text{ mH}$  or  $0.36 \text{ mH}$ .

As shown in Figures 5(c) and (d), the received powers for two receivers are the same when the resonant frequency of  $L_{LCC}C_{LCC}$  tank is equal to  $127 \text{ kHz}$  or  $134 \text{ kHz}$ , respectively. Considering

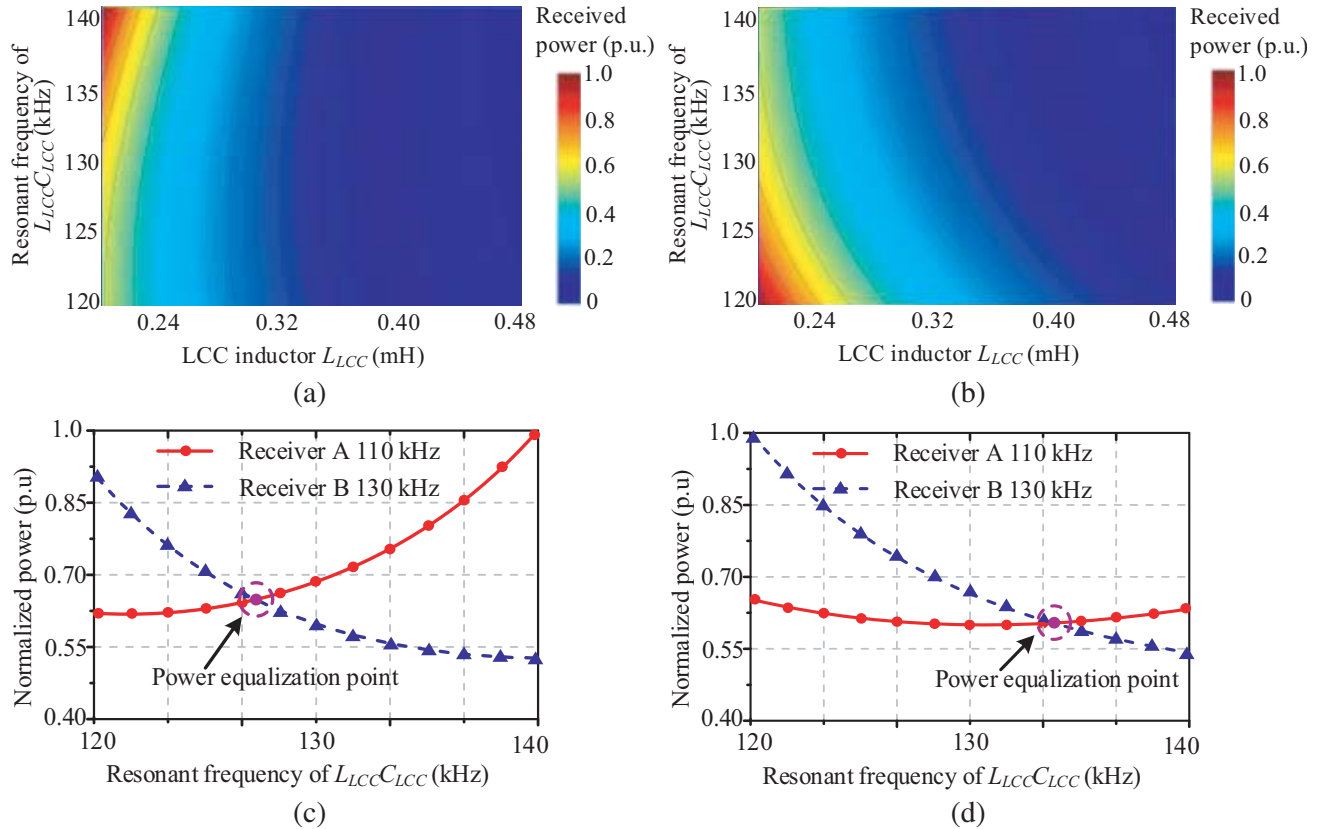


**Figure 5.** Received power of two receivers under different parameters. (a) Receiver A with 110 kHz. (b) Receiver B with 130 kHz. (c) Power distribution with  $0.21 \text{ mH}$   $L_{LCC}$ . (d) Power distribution with  $0.36 \text{ mH}$   $L_{LCC}$ .

the lower resistance, the inductor with 0.21 mH is selected for the LCC compensation. Thus, the capacitances of  $C_T$  and  $C_{LCC}$  can be calculated as 2.7 nF and 7.3 nF. From these results, it can be confirmed that only one transmitter with LCC compensation can effectively provide the same power to different receivers with different resonant frequencies.

### 2.4. BFC and TDM Operation

Since the motor side does not involve any controller or inverter, the motor motion control should be handled at the transmitter side. Based on the property of selective WPT, when the operating frequency of the transmitter is tuned to the resonant frequency of receiver A, then only the receiver A can pick up the wireless power and drive the motor A while the receiver B can pick up nearly no power. Thus, the motor A can be independently energized by setting the operating frequency of the transmitter at  $f_A$ . Similarly, the motor B can be independently energized by setting the operating frequency of the transmitter at  $f_B$ . The two resonant frequencies of  $f_A$  and  $f_B$  are fixed values. When only one motor is needed to be targeted, the corresponding operating frequency of the transmitter should be adopted. In order to provide power control while maintaining the operating frequencies and switching signal duty ratio, the BFC method is employed, namely, the operating frequency of the transmitter is always kept at one of the resonant frequencies. The BFC aims to control the effective number of transmitted cycles  $N_{ei}$  over the total number of cycles  $N_{Ti}$  in a short time section, as shown in Figure 6. The duty ratio of BFC can be expressed as

$$\delta_{BFCi} = \frac{N_{ei}}{N_{Ti}} \times 100\% \tag{13}$$

As the resonant frequency is much higher than the BFC time section of 400  $\mu$ s which includes hundreds of cycles, this control method can offer smooth control of wireless power. When the two motors need to work simultaneously under the multiple-frequency operation, the TDM is adopted to divide the control period into two time sections. The first time section is for the motor A with 200  $\mu$ s and the second time section if for the motor B with the same 200  $\mu$ s. In other words, only the motor A is independently energized by tuning the operating frequency of the transmitter to  $f_A$  in the first time section. Meanwhile, only the motor B is independently energized by tuning the operating frequency of the transmitter to  $f_B$  in the second time section. Since the control period is much shorter than the electrical time constant of motor windings, the two motors work like simultaneous operation.

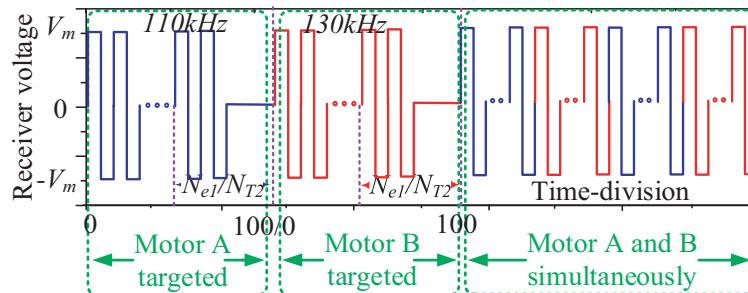


Figure 6. Principle of operation with TDM and BFC.

### 3. SIMULATION AND ANALYSIS

The performance of the proposed wireless coordinative motor drives is simulated by using the finite element analysis software (JMAG). Generally, the total effective flux passes through the pad receiver can be employed to reflect the received current or power transmission ability. Both receiver A and receiver B are independently selected at 110 kHz and 130 kHz to quantitatively analyze the magnetic field distributions.

### 3.1. Finite Element Analysis of Magnetic Field

As shown in Figure 7, both the transmitter and receiver coils adopt the concentrated winding type. It can be found that only one transmitter is needed to serve the two receiver coils. In order to reduce the flux leakage and improve the mutual coupling between the transmitter and the receivers, ferrite bars are adopted at the bottom of the transmitter coil and at the top of the receiver coils. Especially, the ferrite bars of each receiver are only laid on their non-neighboring sides so as to reduce the cross coupling between the two receiver coils. By using finite element analysis, the magnetic flux density above the transmitter coil at different heights are shown in Figure 8.

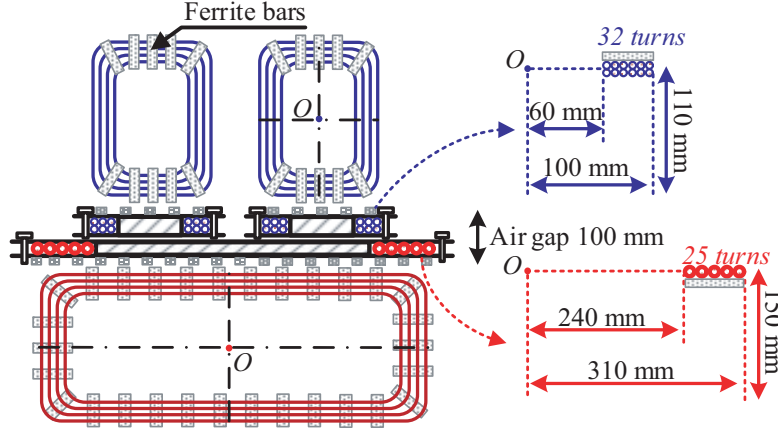


**Figure 7.** Transmitter and receiver coil structures with ferrite bars.

It can be observed that the magnetic flux density distributions at different heights exhibit different shapes and properties. As shown in Figure 8(a), the magnetic flux density at the height of 60 mm has a concave area in the central while the magnetic flux densities at the heights of 100 mm and 150 mm exhibit more uniform distributions as shown in Figures 8(b) and (c). Particularly, the width of uniform magnetic flux distribution at the height of 150 mm is much less than that at the height of 100 mm. As a result, the receiver coils at the height of 100 mm can achieve better tolerance ability of misalignment. Furthermore, the two receivers can achieve almost the same mutual inductance when the receiver position is slightly varied, thanks to the more uniform magnetic flux density distribution.

### 3.2. Independent and Simultaneous Control

As shown in Figure 9(a), when the motor A is targeted, namely, the transmitter is operated at 110 kHz, the magnetic field distribution at the receiver A is much stronger than that at the receiver B, where the magnetic fluxes mainly cluster at the receiver A; when the motor B is targeted, namely, the transmitter is operated at 130 kHz, the magnetic field distribution at the receiver B is much stronger than that at the receiver A as shown in Figure 9(b). Moreover, as shown in Figures 9(c) and (d), the current densities of receivers A and B can be regulated by varying the operating frequency. Thus, it verifies that the proposed wireless motor can be effectively targeted to run by using the selective coupling between the transmitter and receivers.

Moreover, the motor speed control is simulated as depicted in Figure 10. In regions 1 and 2, the motors A and B are individually driven by adopting the BFC duty ratios of 100% and 40%, respectively. In region 3, the two motors are driven simultaneously by both adopting the 50% duty ratio. It verifies that the proposed wireless motors can be effectively controlled for various operating requirements. Moreover, it can be found that the motor speeds of two operating frequencies are almost the same under the duty ratio control. Hence, the power equalization can be effectively achieved by employing LCC compensation.

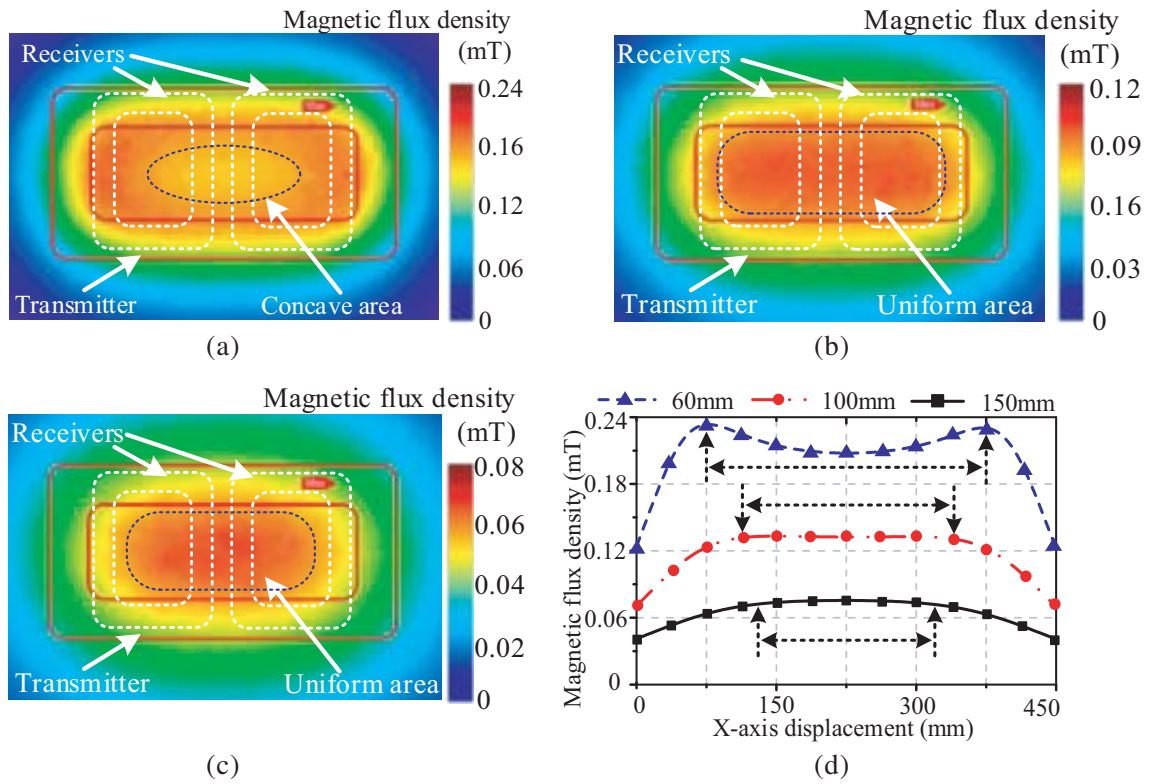


**Figure 8.** Magnetic flux density distributions at different heights. (a) 60 mm height. (b) 100 mm height. (c) 150 mm height. (d) Magnitude distributions at the central plane.

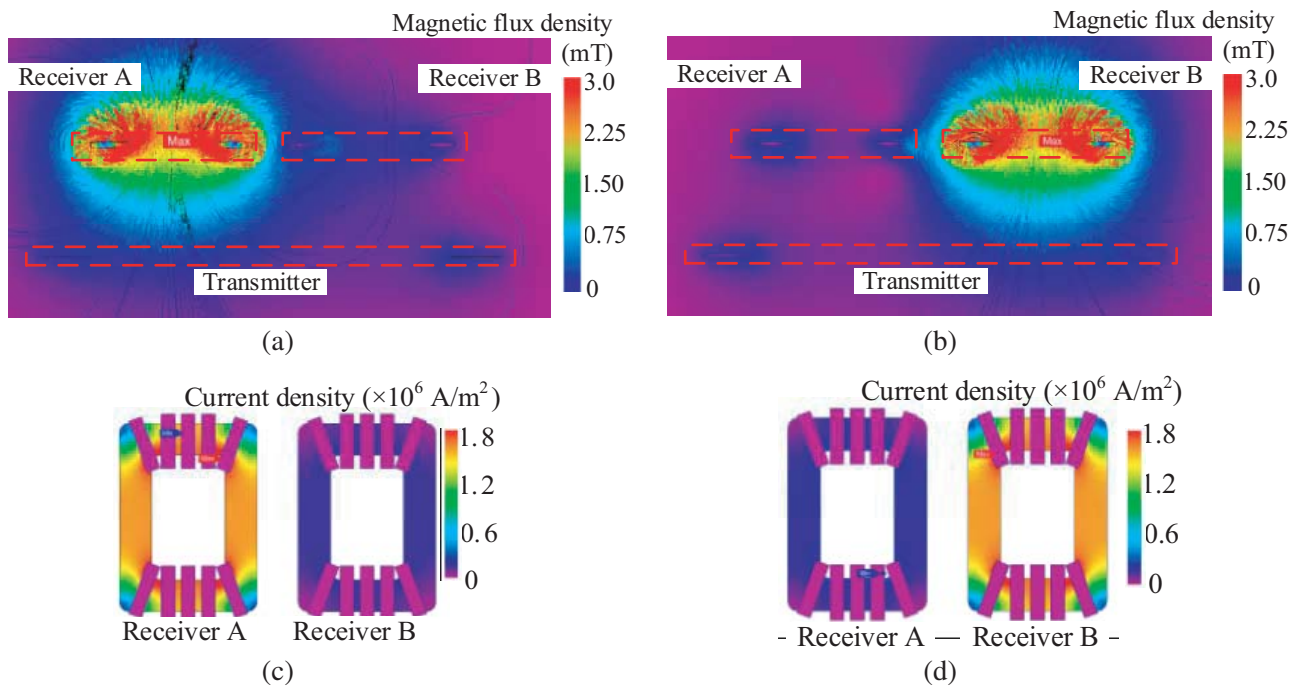


**Figure 9.** Magnetic flux density and current density distributions at different targeted motors. (a) Magnetic flux density when motor A targeted with 110 kHz. (b) Magnetic flux density when motor B targeted with 130 kHz. (c) Current flux density with 110 kHz. (d) Current flux density with 130 kHz.

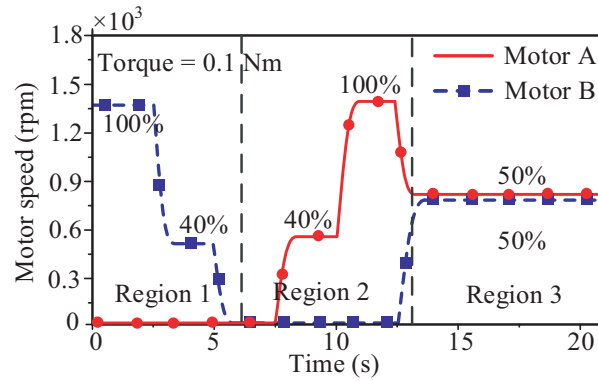


**Figure 10.** Motor speed control characteristics with BFC and TDM control.

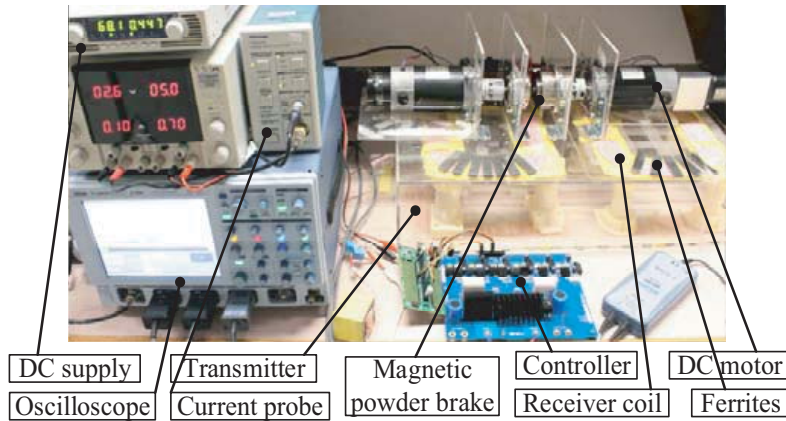


**Figure 11.** Experimental setup of proposed wireless coordinative DC motor drive.

#### 4. EXPERIMENTAL VALIDATION

An experimental prototype has been constructed as shown in Figure 11, in which the KENWOOD PU150-5 and SiC C3M0065090 are used as the DC power supply and inverter switches, the oscilloscope (Lecroy 6100A) is used to display voltages and currents, the currents are measured by CP030 and TCP A300, and the mutual inductance is measured by the LCR meter (ISO-TECH LCR821). The operating frequencies are set at 112 kHz and 134 kHz due to the consideration of practical parameters.

In order to verify the system selectability and power equalization, the currents of the two receivers and motors are measured as shown in Figure 12. It can be observed that when the inverter output is with a peak value of 66 V and the operating frequency is set at 112 kHz, the receiver A and motor A can pick up 1.17 A and 1.0 A, respectively, while the receiver B picks up near no current. At the same inverter output voltage, when the operating frequency is set at 134 kHz, the receiver B and motor B can pick up 1.16 A and 0.98 A while the receiver A picks up near no current. These results well verify that the LCC topology can effectively eliminate the switched-capacitor array and hence provide the multiple-frequency selective WPT operation. Furthermore, the proposed wireless motor drive is well verified to achieve power equalization for the two motors.

Furthermore, by applying the BFC method, the current responses under 40% and 80% duty ratios are measured as shown in Figures 13(a) and (b), respectively. It can be observed that the currents can be effectively chopped by the BFC method. Since the control period of 400  $\mu$ s is much shorter than the natural time constant of DC motor windings, the motor power can be smoothly controlled by the chopped current. As shown in Figure 14(a), the two motors can be independently controlled. Namely, only one motor is targeted to run while another one is idle. By using the TDM scheme, simultaneous

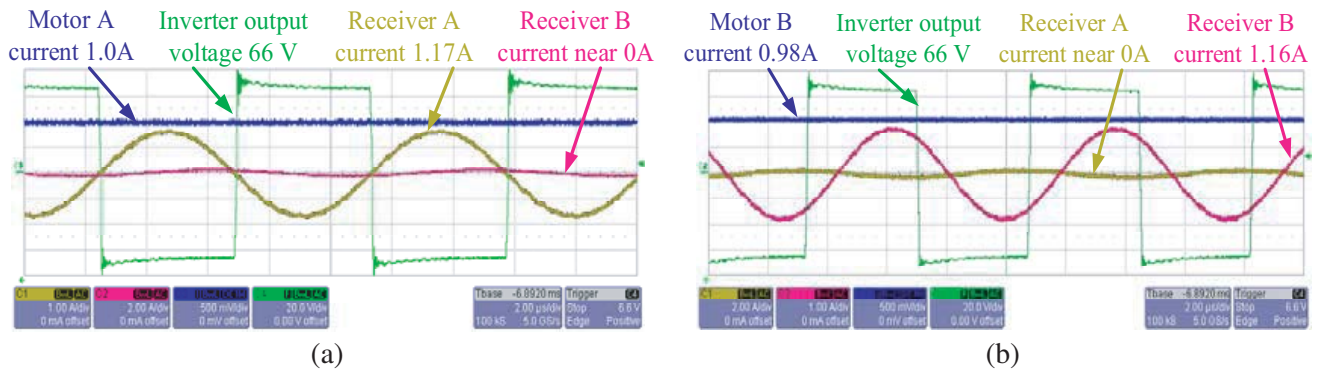


**Figure 12.** Currents of receivers and motors at the same inverter output. (a) With operating frequency of 112 kHz. (b) With operating frequency of 134 kHz.

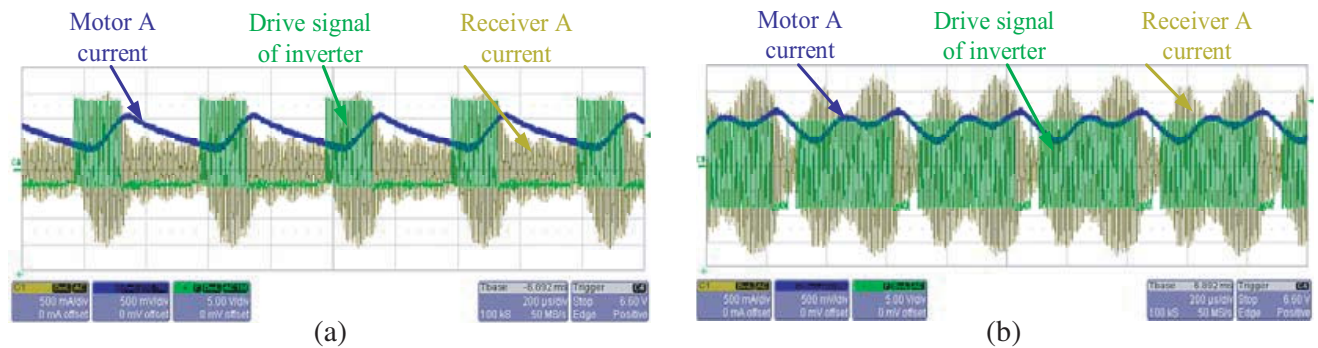


**Figure 13.** Measured waveforms by using BFC method at different duty ratios. (a) With duty ratio of 40%. (b) With duty ratio of 80%.

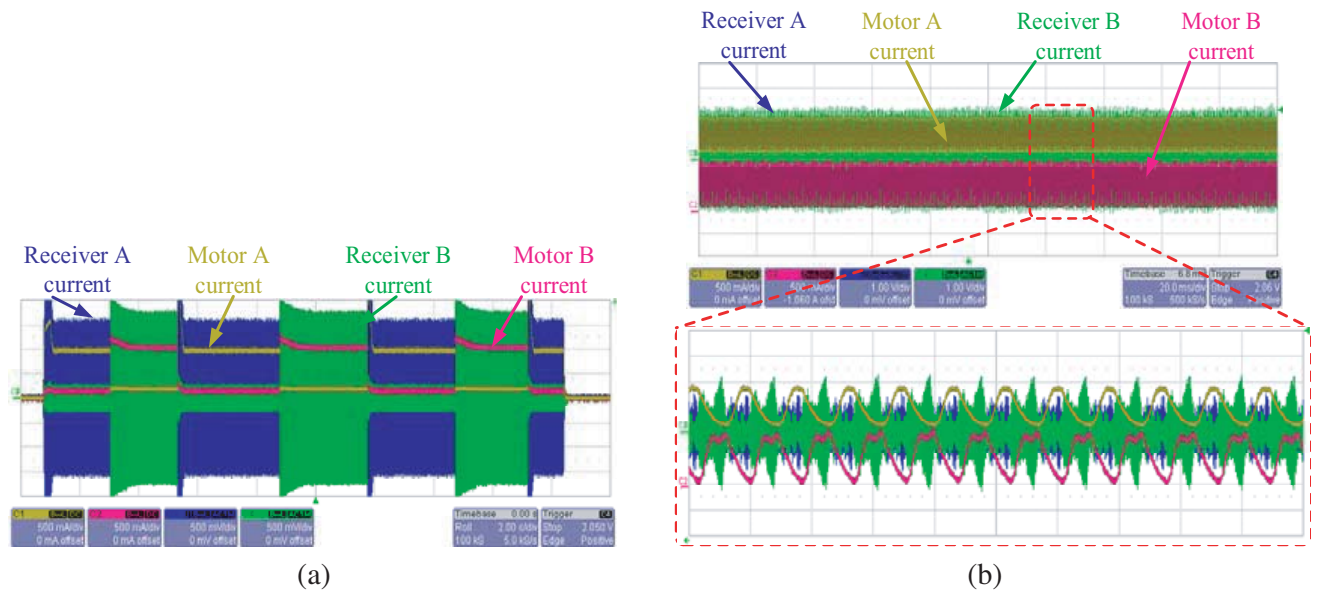


**Figure 14.** Measured current waveforms with different motor operations. (a) Independent motor control. (b) Simultaneous motor control.

motor motions can be achieved as shown in Figure 14(b). It can be found that when both frequencies of 112 kHz and 134 kHz are set at a duty ratio of 50%, the currents of the two motors are produced alternately in a short period of 200  $\mu$ s, which is much shorter than the constant time of DC motor windings. Thus, the motor can be independently and simultaneously operated by combining the BFC and TDM.

Finally, the speed control at different torques is conducted as shown in Figure 15. It can be observed that the motor can be well controlled from 0 rpm to near 1200 rpm with respect to different BFC duty ratios. The BFC can almost provide the desired linear speed control. Moreover, the two motor speeds at the same duty ratio under the same torque are almost the same. Thus, the motors can be independently and also simultaneously controlled by using different frequency combinations.

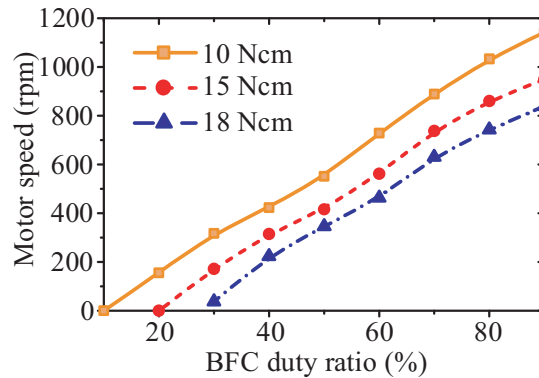


**Figure 15.** Speed control at different torques by using BFC.

## 5. CONCLUSION

In this paper, a novel class of wireless coordinative DC motor drives has been proposed and implemented. Only one transmitter is needed to feed and control multiple PMDC motors without cables. As a result, there will not be any converter or controller at the motor side and hence robustness can be improved. In order to achieve multiple-frequency selective WPT, the LCC compensation is adopted so as to eliminate the switched-capacitor array. By newly employing the TDM scheme and BFC method, it can provide simultaneous and independent WPT to different motors, hence achieving the desired coordinative motion.

## ACKNOWLEDGMENT

This work was supported by a grant (Project No. 17204317) from the Hong Kong Research Grants Council, Hong Kong Special Administrative Region, China.

## REFERENCES

1. Chau, K. T., C. Jiang, and W. Han, "State-of-the-art electromagnetics research in electric and hybrid vehicles," *Progress In Electromagnetics Research*, Vol. 159, 139–157, Oct. 2017.
2. Covic, G. A. and J. T. Boys, "Inductive power transfer," *Proceedings of the IEEE*, Vol. 101, No. 6, 1276–1289, Jun. 2013.
3. Jiang, C., K. T. Chau, C. Liu, and C. H. T. Lee, "An overview of resonant circuits for wireless power transfer," *Energies*, Vol. 10, No. 7, 894:1–20, Jun. 2017.
4. Robichaud, A., M. Boudreault, and D. Deslandes, "Theoretical analysis of resonant wireless power transmission links composed of electrically small loops," *Progress In Electromagnetics Research*, Vol. 143, 485–501, Nov. 2013.

5. Han, W., K. T. Chau, C. Jiang, and W. Liu, "Accurate position detection in wireless power transfer using magnetoresistive sensors for implant applications," *IEEE Transactions on Magnetics*, Vol. 54, No. 11, paper No. 4001205, 1–5, Nov. 2018.
6. Jiang, C., K. T. Chau, C. Liu, C. H. T. Lee, W. Han, and W. Liu, "Move-and-charge system for automatic guided vehicles," *IEEE Transactions on Magnetics*, Vol. 54, No. 11, paper No. 8600105, 1–5, Nov. 2018.
7. Kim, J., H. C. Son, D. H. Kim, and Y. J. Park, "Optimal design of a wireless power transfer system with multiple self-resonators for an LED TV," *IEEE Transactions on Consumer Electronics*, Vol. 58, No. 3, 775–780, Aug. 2012.
8. Saad, M., M. Hannan, A. S. Salina, and H. Aini, "Design of spiral circular coils in wet and dry tissue for bio-implanted micro-system applications," *Progress In Electromagnetics Research M*, Vol. 32, 181–200, Aug. 2013.
9. Hannan, M., M. Saad, A. S. Salina, and H. Aini, "Modulation techniques for biomedical implanted devices and their challenges," *Sensor*, Vol. 12, No. 1, 297–319, Dec. 2012.
10. Mi, C. C., G. Buja, S. Y. Choi, and C. T. Rim, "Modern advances in wireless power transfer systems for roadway powered electric vehicles," *IEEE Transactions on Industrial Electronics*, Vol. 63, No. 10, 6533–6545, Oct. 2016.
11. Liu, W., K. T. Chau, C. H. T. Lee, C. Jiang, and W. Han, "A switched-capacitorless energy-encrypted transmitter for roadway-charging electric vehicles," *IEEE Transactions on Magnetics*, Vol. 54, No. 11, 1–6, Jul. 2018.
12. Kim, J., W. S. Choi, and J. Jeong, "Loop Switching technique for wireless power transfer using magnetic resonance coupling," *Progress In Electromagnetics Research*, Vol. 138, 197–209, Mar. 2013.
13. Han, W., K. T. Chau, Z. Zhang, and C. Jiang, "Single-source multiple-coil homogeneous induction heating," *IEEE Transactions on Magnetics*, Vol. 53, No. 11, paper No. 7207706, 1–6, Nov. 2017.
14. Jiang, C., K. T. Chau, Y. Y. Leung, C. Liu, C. H. T. Lee, and W. Han, "Design and analysis of wireless ballastless fluorescent lighting," *IEEE Transactions on Industrial Electronics*, Vol. 66, No. 5, 4065–4074, May 2019.
15. Chau, K. T., *Electric Vehicle Machines and Drives — Design, Analysis and Application*, Wiley-IEEE Press, Jun. 2015.
16. Poon, A. S. Y., "A general solution to wireless power transfer between two circular loop," *Progress In Electromagnetics Research*, Vol. 148, 171–182, Aug. 2014.
17. Jiang, C., K. T. Chau, W. Han, and W. Liu, "Development of multilayer rectangular coils for multiple-receiver multiple-frequency wireless power transfer," *Progress In Electromagnetics Research*, Vol. 163, 12–24, Aug. 2018.
18. Qiu, C., K. T. Chau, Z. Zhang, and T. W. Ching, "A comparative study of flux cancellation among multiple interconnected modular pads in lumped IPT system," *Progress In Electromagnetics Research M*, Vol. 49, 131–140, Aug. 2016.
19. Badawe, M. E. and O. M. Ramahi, "Efficient metasurface rectenna for electromagnetic wireless power transfer and energy harvesting," *Progress In Electromagnetics Research*, Vol. 161, 35–40, Mar. 2018.
20. Jang, B. J., S. Lee, and H. Yoon, "HF-band wireless power transfer system: Concept, issues, and design," *Progress In Electromagnetics Research*, Vol. 124, 211–231, Jan. 2012.
21. Li, C. J. and H. Ling, "Investigation of wireless power transfer using planarized, capacitor-loaded coupled loops," *Progress In Electromagnetics Research*, Vol. 148, 223–231, Aug. 2014.
22. Badawe, M. E. and O. M. Ramahi, "Efficient metasurface rectenna for electromagnetic wireless power transfer and energy harvesting," *Progress In Electromagnetics Research*, Vol. 161, 35–40, Mar. 2018.
23. Jiang, C., K. T. Chau, T. W. Ching, C. Liu, and W. Han, "Time-division multiplexing wireless power transfer for separately excited DC motor drives," *IEEE Transactions on Magnetics*, Vol. 53, No. 11, paper No. 8205405, 1–5, Nov. 2017.

24. Jiang, C., K. T. Chau, C. Liu, and W. Han, "Design and analysis of wireless switched reluctance motor drives," *IEEE Transactions on Industrial Electronics*, Vol. 66, No. 1, 245–254, Jan. 2019.
25. Zhang, W., S. C. Wong, K. T. Chi, and Q. Chen, "Design for efficiency optimization and voltage controllability of series-series compensated inductive power transfer systems," *IEEE Transactions on Power Electronics*, Vol. 29, No. 1, 191–200, Jan. 2014.
26. Pantic, Z., S. Bai, and S. M. Lukic, "ZCS-compensated resonant inverter for inductive-power-transfer application," *IEEE Transactions on Industrial Electronics*, Vol. 58, No. 8, 3500–3510, Aug. 2011.